

Influence of the underlying terrain on the jitter of astronomic images

V.V. Nosov, V.P. Lukin, and E.V. Nosov

*Institute of Atmospheric Optics,
Siberian Branch of the Russian Academy of Sciences, Tomsk*

Received February 12, 2004

An attempt is made to take into account the effect of the underlying terrain (including the mountain terrain) at the site of astronomic receivers on the variance of the image jitter of extraterrestrial objects. In particular, it is shown that the account of the terrain peculiarities enables one to achieve an agreement between theory and experimental data, which are considerably different from the well known theoretical secant law. The study is carried out based on theoretical calculations and generalization of experimental data. The fact is analyzed that the quality of optical images in ground-based non-adaptive astronomic telescopes is governed by the atmospheric turbulence. Turbulence is a cause of random distortions in the phase front of a light wave propagating from an extraterrestrial source. In astronomy, the image jitter is the factor responsible for the largest error in observations. The allowance made for the terrain allows us to explain the considerable discrepancy between the experimental results and the theoretical secant law.

The quality of optical images in ground-based non-adaptive telescopes is known¹⁻⁵ to be largely determined by the atmospheric turbulence, which induces random distortions into the phase front of a light wave propagating from an extraterrestrial source. In astronomy,^{3,4} the image jitter is a factor contributing most significantly to the error of observations. Since the results of observations are usually recorded on photographic plates, the image displacement during the exposure leads to blurring of the resulting image. The destruction of the inner structure of image is of the second order of smallness in this case.

The jitter is usually characterized by the variance σ_d^2 of linear image displacements in the focal plane. Often angular displacements characterized by the variance of angular displacements σ^2 and the rms deviation of the angular displacements σ are considered in place of linear displacements. The parameters σ_d and σ are related as $\sigma = \sigma_d/F_t$, where F_t is the focal length of the receiving telescope. Qualitatively, the image jitter can be described by fluctuations of the arrival angles^{1,2} on the base equal to the diameter of the receiving telescope. V.I. Tatarskii was the first to consider theoretically the variance of image jitter of a plane wave in the stronger approximation of wave optics.¹ For the variance σ^2 (along both of the transverse coordinates), the following equation was obtained in Ref. 1:

$$\sigma^2 = 4.51 a_t^{-1/3} I_0, \text{ rad}^2, I_0 = \sec \theta \int_0^\infty C_n^2(h) dh, \quad (1)$$

where a_t is the radius of the entrance aperture of the telescope; θ is the zenith angle of the observed object

(measured from the zenith direction at the place of receiver's location); $C_n^2(h)$ is the structure characteristic of fluctuations of the refractive index of the air, depending on the height h above the surface (the vertical profile of C_n^2). For every value of the angle θ , the value of I_0 in Eq. (1) determines the integral intensity of atmospheric turbulence along the optical paths of a given slope.

Equation (1) was subjected to serious experimental testing.^{2-4,7-9} The experiments were mostly conducted along paths with extraterrestrial sources^{3,4} and, in the smaller number, along near-surface paths.^{2,7-9} As a result, it was found that in astronomic observations the experimental values of the variance σ^2 in the most cases are close to the theoretical ones. However, quite often significant deviations from the secant law³

$$\sigma^2 \sim \sec \theta. \quad (2)$$

following from Eq. (1) were observed as well.

These deviations generated a long discussion among experimental astronomers (starting from 1957–1959 [Ref. 3]) and served as a cause for a great number of the experimental dependences of the jitter variance on the zenith angle θ , which were different for every observation site.

The discrepancy between the measured and calculated values was also noted in the experiments along the near-surface paths,⁷⁻⁹ and then it was explained theoretically¹⁰ by the fact that the waves used in Refs. 7–9 were other than plane.

The discrepancies revealed between the experimental and theoretical data stimulated development of new theoretical approaches to description of image jitter in

order to predict the effect of the factors ignored by Eq. (1). For example, the approaches accounting for the effect of spatial boundedness of the received wave (which is equivalent to application of optical beams) and the effect of the outer scale of turbulence (the strong dependence on the outer scale of turbulence was demonstrated by the results on the displacements of laser beams propagating along the surface paths^{11–14}).

The first results on the account of the spatial boundedness of the wave⁶ concerned the variance of the arrival angles and were valid under conditions, at which the beam propagated almost without broadening. In the approximation of wave optics, the variance of image jitter of laser sources is considered in Ref. 10, where the variance equation suitable for sources with arbitrary coherence and divergence was derived. This equation is valid for any turbulence intensity and accounts for the effect of the outer scale of turbulence. In the extreme cases, the well-known theoretical results^{1,6} follow from Ref. 10. The conclusions drawn based on this equation agree with the experiments for the laser beams propagating along horizontal surface paths.^{7–9} In Ref. 15, the results of Ref. 10 were generalized to the case of inhomogeneous optical paths of arbitrary geometry. Based on the approach developed in Ref. 10, the equations were derived for the space and time correlation functions of the image jitter,^{15,16} as well as for the frequency spectra.^{15,17} The calculation of the variance of image jitter using the approach developed in Refs. 18 and 19 confirmed the conclusions of Ref. 10 and predicted the influence of the deviation of the image plane in the receiver from the focal plane.

For natural extraterrestrial optical sources, the results of the theoretical and experimental studies give the following equation for the variance of angular displacements of images σ^2 at the paths of arbitrary geometry^{10,15}:

$$\sigma^2 = 4.1 a_t^{-1/3} I, \quad (3)$$

$$I = \int_0^x dx' C_n^2[h(x')] (x'/x)^2 \{(x'/x)^{-1/3} - [(x'/x)^2 + L_0^2[h(x')]/(2\pi^2 a_t^2)]^{-1/6}\},$$

where x is the optical path length; a_t is the radius of the entrance aperture of the receiving telescope; $C_n^2(h)$ and $L_0(h)$ are the vertical profiles of the structure characteristic of fluctuations of the refractive index and the outer scale of turbulence; $h(x')$ is the height of the current point along the optical path above the surface at the distance x' from the source (current path height); x' is the current path length measured from the source.

As known, at the heights above the surface layer, whose thickness is several kilometers, the function $C_n^2(h)$ differs from zero only slightly. Therefore, in the region significant for integration in Eq. (3), the inequality $h(x') \leq h_{\text{eff}}$ is fulfilled, where h_{eff} is the effective thickness of the optically active atmospheric layer. This condition imposes restrictions on the range

of variation of the current path length x' and allows further simplification. Representing the current path height as¹ $h(x') \approx (x - x') \cos \theta$, we find that in Eq. (3) the ratio x'/x is very close to unity. The corrections arising in Eq. (3) at replacement $x'/x \rightarrow 1$ are on the order of $h_{\text{eff}}/(x \cos \theta)$, and for the astronomic paths they are within hundredth parts of percent. As a result, for the variance of jitter of astronomic images we obtain

$$\sigma^2 = 4.1 a_t^{-1/3} I, \quad (4)$$

$$I = \int_0^x dx' C_n^2[h(x')] \{1 - [1 + L_0^2[h(x')]/(2\pi^2 a_t^2)]^{-1/6}\}.$$

As can be seen from the comparison of Eqs. (4) and (1), within the framework of the approximations¹ ($L_0(h) = \infty$, $h(x') = (x - x') \cos \theta$) taken in Ref. 1, the equality $I = I_0$ is fulfilled and Eq. (4) differs from Eq. (1) only by a numerical coefficient. This difference is insignificant (about 9%) and caused by the Gaussian approximation used for the transmission function of the entrance pupil of the receiving telescope when deriving Eq. (3).

Equation (4) accounts for the effect of the vertical profile of the outer scale of turbulence and imposes no restrictions on the function describing the current path height. As follows from Eq. (4), to predict the jitter variance, it is necessary to set the vertical profiles of the turbulence intensity $C_n^2(h)$ and the outer scale of turbulence $L_0(h)$, as well as to determine the current path height $h(x')$ to take into account the underlying terrain.

The available theoretical and experimental data for the vertical models of the structure characteristic $C_n^2(h)$ were reviewed in Refs. 2 and 20, and it was recommended to use smoothed experimental profiles in practice. One of them is the profile proposed in Ref. 2:

$$C_n^2(h) = C_n^2(h_*) (h/h_*)^{-2/3} \exp[-(h - h_*)/h_{\text{eff}}], \quad (5)$$

where $h_{\text{eff}} = 3200$ m is the effective thickness of the active atmospheric layer; $h_* = 2.5$ m is the characteristic height of C_n^2 measurements in the surface layer. At the surface values of $C_n^2(h_*)$ set properly, the profile (5) agrees with other smoothed models and allows satisfactory description of the experimental data.

To further simplify Eq. (4), estimate first the effect of the outer scale of turbulence on the variance of image jitter. To do this, apply the known vertical models of the outer scale in Eq. (4). According to the data of Ref. 5, for the height $h \geq 1$ m we have:

1. $L_0(h) = \kappa h$, $\kappa = 0.4$; $L_0(h)$, m, h , m;
2. $L_0(h) = \kappa h$, $0 \leq h \leq h_1$;
 $L_0(h) = 2\sqrt{h}$, $h > h_1$; $h_1 = 25$ m;
3. $L_0(h) = \kappa h$, $0 \leq h \leq h_1$;
 $L_0(h) = 2\sqrt{h}$, $h_1 < h \leq h_2$;
 $L_0(h) = 2\sqrt{h_2}$, $h > h_2$; $h_2 = 1000$ m;

4. $L_0(h) = (\kappa h + \kappa_1 h^2) \exp(-\kappa_2 h) + f(h)$,
 $f(h) = 5 [1 + (h - h_3)^2/h_4^2]^{-1}$,
5. $L_0(h) = f(h)$, $h_3 = 7500$ m, $h_4 = 2000$ m,
 $\kappa_1 = 0.057$, $\kappa_2 = 0.042$.

The Karman model 1 is applicable to the surface layer,¹ the model 2 was proposed by D. Fried⁵; and the model 3 is a generalization of the models 1 and 2. The model 5 was obtained from the measurements conducted in the mountain observatories of the USA, France, and Chili⁵ at the tops of isolated mountains. The model 4 was constructed based on the measurement results obtained in the mountain-valley region of the USA²¹ up to the heights of 5–7 km; at high altitudes the model 4 coincides with the model 5.

The calculation of the jitter variance by Eq. (4) using the models (5) and (6) in the case of a plain terrain, when the current path height $h(x')$ can be presented in the form

$$h(x') = h_0 + (x - x') \cos \theta,$$

where h_0 is the height of the center of the receiver's aperture above the surface, shows that at the same surface values of $C_n^2(h_*)$ the different vertical models of the outer scale give different values of the variance σ^2 . At the same time, for any zenith angle θ from the range $0 \leq \theta \leq 89^\circ$, the variance σ^2 normalized to its value σ_0^2 at $\theta = 0^\circ$ is almost independent of the model of the outer scale. This allows us, applying the mean-value theorem, to remove the corresponding factor from the integral sign in Eq. (4) and present the jitter variance in the form

$$\sigma^2 = 4.1 a_t^{-1/3} \mu \int_0^x dx' C_n^2 [h(x')],$$

$$\mu = 1 - [1 + (L_0^{\text{eff}})^2 / (2\pi^2 a_t^2)]^{-1/6}, \quad x \rightarrow \infty, \quad (7)$$

where L_0^{eff} is the effective outer scale of turbulence characterizing the turbulence along the entire path. The values of the effective outer scale of turbulence L_0^{eff} are shown in Fig. 1 for different vertical models of $L_0(h)$. For each model, Fig. 1 gives the range of variation of L_0^{eff} at the height of the receiving aperture h_0 varying in the interval $h_0 = 3\text{--}48$ m typical of the most ground-based astronomic telescopes. The value of L_0^{eff} is calculated for a telescope with 0.5-m radius of the primary mirror. The variation of the radius in the range $a_t = 0.1\text{--}3$ m allowable for real telescopes gives the error in determination of L_0^{eff} with the upper boundary of 30% for the models 1–3 and 50% for the models 4–5.

In Eq. (7), the value of μ characterizes the degree of reduction of the jitter variance for the reason that real outer scale of turbulence is different than infinity. As follows from the data shown in Fig. 1, for each of the $L_0(h)$ models the value of $\mu^{1/2}$ varies within 0.79–0.88 for the model 1, 0.76–0.80 for the model 2, 0.75–0.79 for the model 3, 0.37–0.30 for

the model 4, and 0.13–0.14 for the model 5. So it can be seen that the allowance for the real profiles of the outer scale of turbulence can lead to a tenfold reduction of the root-mean-square deviation of jitter.

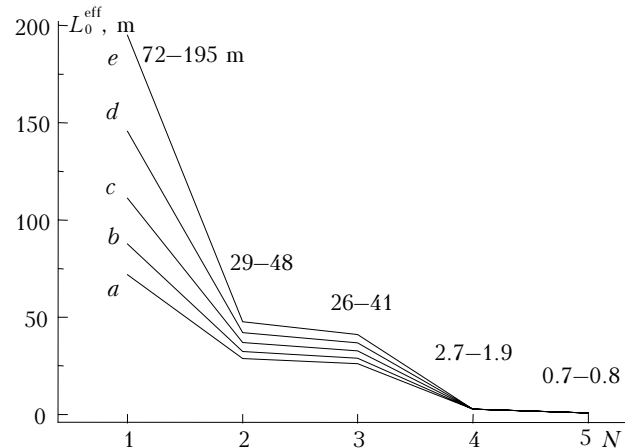


Fig. 1. Effective outer scale of turbulence for different vertical profiles of the outer scale (6). Plain surface, $a_t = 0.5$ m; N is the number of the model in Eq. (6); $h_0 = 3$ (a), 6 (b), 12 (c), 24 (d), 48 m (e).

The effective outer scale of turbulence was obtained in Ref. 22 from the calculated structure function of phase fluctuations (with the Karman model of the turbulence spectrum). The calculations have been made using different methods for the vertical profiles of the outer scale of turbulence, corresponding to the models 2, 3, and 5 in Eq. (6), at the zero value of h_0 using different models of $C_n^2(h)$. If we average the values of the outer scale of turbulence obtained in Ref. 22 by all the methods of calculation and the profiles of $C_n^2(h)$ used, then we obtain the following values for the averaged effective outer scale $\langle L_0^{\text{eff}} \rangle$: $\langle L_0^{\text{eff}} \rangle = 64$ m for the model 2, $\langle L_0^{\text{eff}} \rangle = 43$ m for the model 3, $\langle L_0^{\text{eff}} \rangle = 1$ m for the model 5.

According to Ref. 11, the Karman outer scale $\langle L_0^{\text{eff}} \rangle$ and the "exponential" scale L_0^{eff} entering the Eq. (7) are related as $\langle L_0^{\text{eff}} \rangle = 1.8 L_0^{\text{eff}}$. With the allowance for this relation, the comparison of the L_0^{eff} values shown in Fig. 1 (at $h_0 = 3$ m) with the $\langle L_0^{\text{eff}} \rangle$ values shows that they almost coincide (the difference does not exceed 20%).

As can be seen from Fig. 1, the effective outer scale of turbulence has a marked dependence on the receiver's height above the surface h_0 . However, this height is often assumed zero. The estimates show that the relative error in the jitter variance due to the replacement of the real receiver's height h_0 by zero ($h_0 = 0$) is on the order of $(h_0/h_{\text{eff}})^{1/3}$. This error becomes noticeable for large ground-based telescopes, in which the center of the entrance mirror (lens) is usually located at the height of several tens of meters from the surface. For example, for the receiver's height of 25 m ($h_0 = 25$ m) the error is 20%. Consequently, in more accurate calculations it is necessary to take the receiver's height h_0 into account.

To reduce the atmospheric effect, astronomic telescopes are usually installed highlands, including mountain tops. In this case, the optical path usually passes over the surface parts with uneven or rugged terrain. Therefore, the current path height $h(x')$ should be specified taking the underlying terrain into account.

Introduce the function describing the surface height above the sea level (terrain amplitude). In the general case, this function depends on two coordinates on the globe surface. However, we need to know this function only along the projection of the optical path onto the surface. Let $P(s)$ denote the height of the ground above the sea level along a circle of the large Earth's radius, which is obtained as the globe is crossed by a plane passing through its center and both ends of the optical path. The argument of the function $P(s)$ is the arc length of the circle of the large Earth's radius $s = s(x')$, $0 \leq x' \leq x$ (x' is measured from the source). If the arc length $s(x')$ is measured from the receiver (near which $x' = x$), then $s(x) = 0$ and $0 = s(x) \leq s(x') \leq s(0)$. As the arc length s changes, the function $P(s)$ can be both positive and negative (terrain amplitude above and below the sea level). In this case $P[s(x)] = P(0) = P_0$ and $P[s(0)]$ are the ground heights above the sea level at the point of the telescope location and under the observed object (Fig. 2). The condition $P[s(x')] = \text{const}$ corresponds to the plain terrain.

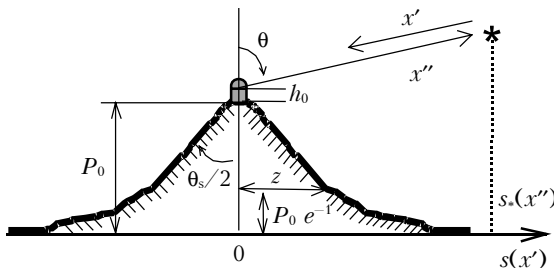


Fig. 2. Observation geometry.

With the allowance made for the above definitions, the current height $h(x')$ depending on the underlying terrain can be represented as follows:

$$h(x') = -R - P[s(x')] + \{[h_0 + P[s(x)] + R]^2 + (x - x')^2 + 2(x - x')[h_0 + P[s(x)] + R] \cos \theta\}^{1/2},$$

where R is the Earth's radius. The current arc length $s(x')$ is equal to the Earth's radius R multiplied by the central angle $\alpha(x', x)$ between two points of the current path x and x' : $s(x') = R\alpha(x', x)$.

The angle $\alpha(x', x)$ can be easily determined and for $0 \leq \theta \leq \pi$ is equal to

$$\alpha(x', x) = \arctan \left(\frac{(x - x') \sin \theta}{h_0 + P[s(x)] + R + (x - x') \cos \theta} \right).$$

Since $h(x') \leq h_{\text{eff}}$ in the region significant for integration in Eq. (7), the last equations can be simplified through expansion into a power series over small parameter $|x - x'|/R$. Restricting our consideration to the first terms of the expansion, we obtain

$$h(x') = h_0 + P(0) - P[s(x')] + (x - x') \cos \theta + (x - x')^2 \sin^2 \theta / (2R),$$

$$s(x') = (x - x') \sin \theta - (x - x')^2 \sin (2\theta) / (2R).$$

The last terms in these equations account for the mean curvature of the surface due to the Earth's sphericity. For almost all slant paths, these parameters are small as compared to the previous ones and can be usually neglected. They turn out significant only for the close-to-horizontal paths, when the zenith angles of the observed objects θ are near $\theta = \pi/2$. The estimates show that the last terms should be necessarily taken into account in a narrow range of zenith angles: $90^\circ - \delta \leq \theta \leq 90^\circ + \delta$, where $\delta \approx 0.9^\circ$. Since the observations of astronomic objects located just near the horizon are not usually conducted, for all real zenith angles ($0^\circ \leq \theta \leq 89^\circ$) we have

$$h(x') = h_0 + P[s(x)] - P[s(x')] + (x - x') \cos \theta,$$

$$s(x') = (x - x') \sin \theta, \quad s(x) = 0.$$

Since the integrals in Eqs. (4) and (7) are invariant with respect to the change of variables $x - x' \rightarrow x''$ (the new variable x'' , unlike x , is measured from the receiver, see Fig. 2), it is convenient to use in calculations $h_*(x'')$ and $s_*(x'')$, determined as $h_*(x'') = h(x - x'')$, $s_*(x'') = s(x - x'')$, in place of $h(x')$ and $s(x')$, and then

$$h_*(x'') = h_0 + P(0) - P[s_*(x'')] + x'' \cos \theta,$$

$$s_*(x'') = x'' \sin \theta, \tag{8}$$

$$0 = s_*(0) \leq s_*(x'') \leq s_*(x), \quad 0 \leq x'' \leq x.$$

To study the effect of the underlying terrain on the jitter of astronomic images, we have to set the function $P(s_*)$ simulating the mountain terrain with the telescope located at a mountain top. However, if the telescope is located on top of an isolated mountain, the calculations involve simple function $P(s_*)$ specifying the terrain of a single mountain,

$$P(s_*) = P_0 \exp[-(s_*/z)^n], \quad n = \text{const}, \tag{9}$$

$$s_* \geq 0, \quad P(0) = P_0.$$

Here P_0 is the mountain height; z is the level $1/e$ half-width of the mountain base. If the level $1/e$ cross section of the mountain is called its foot, then z is the foot radius. The constant n in Eq. (9) characterizes the steepness of the mountain slope near the telescope. It is clear that the highest steepness of the slope near the telescope corresponds to the small n values ($n < 1$). The lowest steepness of the slope near the telescope takes place at large n ($n \rightarrow \infty$), when the volume profile of the mountain transforms into a cylinder. To estimate the effect of the ambient mountain terrain on the image jitter in the telescope located at the top of a mountain, the superposition of the following functions is used

$$P(s_*) = P_0 \exp[-(s_*/z_0)^{n_0}] + \sum_{1 \leq j \leq M} P_{0j} \exp(-[|s_* - s_{*j}|/z_j]^{n_j}), \quad s_*, s_{*j} \geq 0,$$

where P_0 , z_0 , n_0 are, respectively, the height, base half-width (foot radius), and the degree of the slope steepness of the mountain, at whose top the telescope is installed; P_{0j} , z_j , n_j , and s_{*j} are, respectively, the height, base half-width, degree of the slope steepness, and the coordinates of the top (the value of the arc length corresponding to the top) of the neighboring mountain with the number j , M is the number of the considered neighboring mountains located under the optical path in series starting from the mountain, at which the telescope is located ($0 \leq s_{*j} \leq s_{*j+1}$, $1 \leq j \leq M$).

Figure 3 depicts the root-mean-square deviation of the angular image displacements σ normalized to its value σ_0 at $\theta = 0^\circ$ ($\sigma_0 = \sigma$ at $\theta = 0^\circ$) as a function of the zenith angle of the observed astronomic object for different degree of the slope steepness of a single mountain (different values of the parameter n in Eq. (9) at the fixed parameters P_0 and z). As can be seen from Fig. 3, at $\theta \neq 0^\circ$ with the increase of the slope steepness (decrease of n) the image displacements are much smaller as compared to the case of the observed object located in zenith ($\theta = 0^\circ$). This can be explained by the fact that, at the same value of the zenith angle, the length of the part of the optical path located within the optically active atmospheric layer decreases with the increase of the slope steepness.

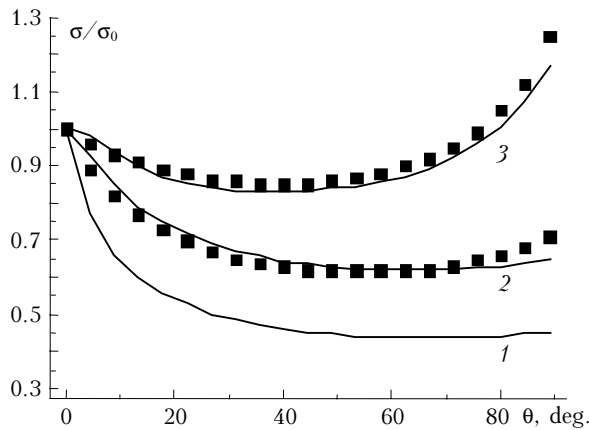


Fig. 3. Normalized root-mean-square deviation of the image jitter vs. the slope steepness of a single mountain. $P_0 = 5$ km, $z = 0.5$ km, $h_0 = 20$ m; $n = 1$ (1), 2 (2), 8 (3). Dots near the curves 2 and 3 show the equivalent dependences corresponding to the exponential profile $n = 1$ and calculated at $z = 1.4$ km (for profile 2, $n = 2$) and $z = 4.6$ km (for profile 3, $n = 8$).

The calculations made for different n show that at $n \neq 1$ the mountain profile (9) can be replaced by the equivalent "exponential" profile, for which $n = 1$. The equivalent profile includes different base half-width z_{equ} . Thus, if $z = 0.5$ km for $n = 1$, then $z_{\text{equ}} = 1.4$ km for $n = 2$, $z_{\text{equ}} = 3.3$ km for $n = 4$, $z_{\text{equ}} = 4.6$ km for $n = 8$, and $z_{\text{equ}} = 0.25$ km for $n = 1/2$.

For the approximate estimates we can assume $z_{\text{equ}} \approx nz_n$. Then we have

$$P_n(s_*) \approx P_{\text{equ}}(s_*),$$

where

$$P_n(s_*) = P_0 \exp[-(s_*/z_n)^n],$$

$$P_{\text{equ}}(s_*) = P_0 \exp[-s_*/z_{\text{equ}}].$$

For the exponential profile of a single mountain, the dependence of σ/σ_0 on the slope steepness is illustrated in Fig. 4. For the data shown in Fig. 4, the slope steepness varies due to the change of the mountain height P_0 and the foot radius z . The ratio of these parameters z/P_0 characterizes the angle $2\theta_s$ formed at the top by the opposite mountain slopes, $\tan \theta_s = z/P_0$ (see Fig. 2). With the decrease of this angle, the slope steepness increases. As follows from Fig. 4, the increase of the slope steepness (decrease of the angle θ_s) results in a significant decrease of the ratio σ/σ_0 . The observed situation is similar to the case considered in Fig. 3. However, here the vertex angle θ_s is not the only parameter determining the value of σ/σ_0 . This can be seen from the comparison of the curves 3 and 4 in Fig. 4, for which the angle θ_s has the same value. The additional parameter is the ratio of the mountain height to the thickness of the optically active atmospheric layer P_0/h_{eff} . According to Fig. 4, for two mountains with the identical profiles but different heights, the parts of the optical path lying within the active atmospheric layer at $\theta \neq 0^\circ$ have different length.

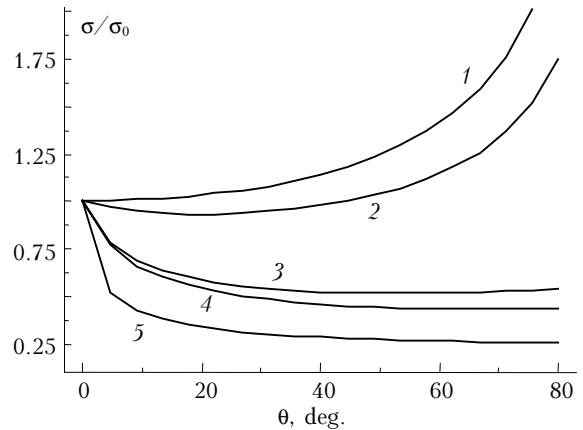


Fig. 4. Normalized root-mean-square deviation of image jitter vs. the slope steepness of a single mountain with the exponential profile (profile (9), $n = 1$) $P(s_*) = P_0 \exp(-s_*/z)$, $h_0 = 20$ m; $P_0 = 0$ km ($\tan \theta_s = \infty$, $\sigma^2/\sigma_0^2 = \sec^2 \theta$) (1), $P_0 = 0.5$ km, $z = 0.5$ km ($\tan \theta_s = 1$) (2), $P_0 = 3$ km, $z = 0.3$ km ($\tan \theta_s = 0.1$) (3), $P_0 = 5$ km, $z = 0.5$ km ($\tan \theta_s = 0.1$) (4), $P_0 = 5$ km, $z = 0.1$ km ($\tan \theta_s = 0.02$) (5).

In the case of an isolated mountain with the exponential profile for the normalized variance of the image jitter σ^2/σ_0^2 , we can obtain a simple approximate equation

$$\sigma^2/\sigma_0^2 = [1 - v m(\xi)]/\cos \theta, \quad (10)$$

$$m(\xi) = \xi (1 + \xi^2)^{-1/6}, \quad \xi = v^{-1} \beta/(\beta + 1),$$

$$v = P_0/h_{\text{eff}}, \beta = \tan(\theta) P_0/z = \tan(\theta)/\tan(\theta_s).$$

As follows from Eq. (10), two complex parameters that determine the value of σ/σ_0 are the ratios $v = P_0/h_{\text{eff}}$ and $\beta = \tan(\theta)/\tan(\theta_s)$. The normalized variance σ^2/σ_0^2 calculated by Eq. (10) within the error of 10% coincides with the numerical results shown in Fig. 4 in the following ranges of the zenith angle: $0 \leq \theta \leq 89^\circ$ for curve 1, $0 \leq \theta \leq 85^\circ$ for curve 2, $0 \leq \theta \leq 65^\circ$ for curves 3 and 4, $0 \leq \theta \leq 45^\circ$ for curve 5.

Figure 5 shows the calculated results on the normalized rms deviation of image jitter for the system of two neighboring mountains. The profile of the mountain system is specified as a sum of two exponential profiles

$$P(s_*) = P_0 \exp(-s_*/z_0) + P_1 \exp(-|s_* - s_{*1}|/z_1), \quad (11)$$

where P_0 , z_0 and P_1 , z_1 are the heights and the foot radii of the mountains, at whose top astronomic receivers are installed, and the neighboring mountain; s_{*1} is the separation between the mountains. At the same height of the mountain, at which the telescope is installed ($P_0 = 3$ km), we have considered different versions of the slope steepness (due to variation of the base half-width z_0). Thus, the group of curves *a* in Fig. 5 corresponds to the high steepness ($\tan \theta_{s_0} = z_0/P_0 = 0.1$, $z_0 = 0.3$ km), while the group *b* corresponds to the moderate steepness ($\tan \theta_{s_0} = z_0/P_0 = 1$, $z_0 = 3$ km). Curves 1–5 (group *a*) and 6–10 (group *b*) in Fig. 5 characterize different versions of the height and location of the neighboring mountain.

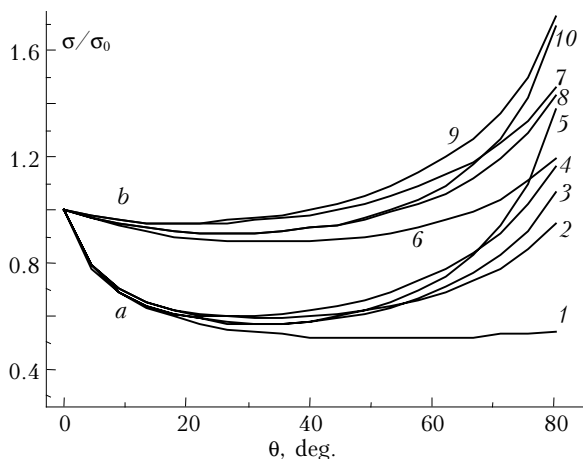


Fig. 5. Normalized rms deviation of image jitter for the system of two mountains; $h_0 = 20$ m, groups *a* and *b* correspond to different versions of the mountain, at which the telescope is installed: (*a*) mountain with highly steep slopes: $P_0 = 3$ km, $z_0 = 0.3$ km; (*b*) mountain with moderately steep slopes: $P_0 = 3$ km, $z_0 = 3$ km.

As can be seen from Fig. 5, the increase of the slope steepness of the mountain, at whose top the telescope is installed, (transition from group *b* to

group *a*) leads to a significant decrease of the ratio σ/σ_0 . In this case, in the first part of the whole range of the zenith angles ($0^\circ \leq \theta \leq 30\text{--}40^\circ$), the mountain system almost does not differ from the case of a single (isolated) mountain. Significant differences arise in the second part of the range ($30\text{--}40^\circ \leq \theta \leq 89^\circ$). In this case, the mountain system causes a considerable increase in the image jitter as compared to the case of a single mountain. The neighboring mountain begins to show its influence, because the optical path crosses the zone of the perturbed atmosphere above the neighboring mountain. In general, the length of the path part lying inside the active atmospheric layer increase, which results in the increase of the jitter variance.

It also follows from Fig. 5 that the decrease of the height and the base half-width of the neighboring mountain leads to a decrease of its effect on the image jitter. The effect of single neighboring mountains depends on the distance they are spaced from the telescope (the main mountain). The mountains located near the telescope exert stronger influence on the image jitter in the central part of the range of the zenith angles ($30\text{--}40^\circ \leq \theta \leq 60\text{--}70^\circ$). As the separation between the neighboring mountain and the telescope increases, its effect shifts from the central part to the range of large zenith angles ($70\text{--}80^\circ \leq \theta \leq 89^\circ$).

Let us compare the obtained theoretical results with the experiment. A lot of experimental data on the image jitter of astronomic objects are available by now.^{23–33} Of greatest interest for a comparison with the theory are the measurements that deviate significantly from the secant law (2). We took the results obtained in Ref. 23 as such data. In Ref. 23 the measurements were conducted at Mount Sanglok in Tajikistan. Mount Sanglok (2237 m above the sea level) is located at about 60 km southeast from Dushanbe, the capital of Tajikistan.

The measurements were conducted in the summer period of 1960. The telescope was installed at the height $h_0 \approx 20$ m from the surface. The mountain, at which the telescope was installed, was not steep on the average. If we represent the mean mountain profile as a triangle with the vertex angle $\langle \theta_s \rangle$ and the foot radius $\langle z \rangle$ (at the level $1/e$), then $\langle z \rangle \approx 2500$ m and $\langle \theta_s \rangle \approx 50\text{--}60^\circ$. At the same time, the mountain had strongly rugged sides. Thus, at the top there was a plateau slightly lowering to the sides (the slope angle $5\text{--}12^\circ$) with the diameter of about 300 m. Outside the plateau, the mountain has high steepness of the slope, which is abrupt at some places. Farther down along the slope, starting from the distance of several hundred meters, neighboring mountains are located. They are quite sharp and decrease in height with the distance from the telescope. The height of the highest neighboring mountain is lower than that of the principal one. All the neighboring mountains form the rugged slope of Mount Sanglok. Consequently, the slope of Mount Sanglok in the sector of observation can be represented as a set including the principal mountain, at which the telescope is installed, and the neighboring mountains. The non-averaged mountain

profile adjacent to the telescope can be considered as a profile of the principal mountain. In approximation of this profile by Eq. (9) corresponding to a single mountain, we can assume $z \approx 250$ m, $n \approx 1.6$. In this case

$$\tan \theta_s \approx z/[P_0 (1 - 1/e)] \approx 0.18 \text{ and } \theta_s \approx 10^\circ.$$

From the data presented in Fig. 5 it follows that for not very large zenith angles ($0 \leq \theta \leq 60\text{--}70^\circ$) the low and sharp neighboring mountains do not contribute markedly to the jitter of astronomic images. Therefore, in comparison of the theory with the experiment, we can neglect the effect of the remote neighboring mountains, restricting our consideration to the case of a single neighboring mountain. Then the profile of the mountain system can be presented as

$$\begin{aligned} P(s_*) &= P_0(s_*) \text{ at } 0 \leq s_* \leq S_*; \\ (s_*) &= P_1(s_*) \text{ at } s_* \geq S_*, \\ P_0(s_*) &= P_0 \exp[-(s_*/z_0)^{n_0}], \\ P_1(s_*) &= P_1 \exp(-[|s_* - s_{*1}|/z_1]^{n_1}), \end{aligned} \quad (12)$$

where S_* is the arc corresponding to the point of intersection of the profiles $P_0(s_*)$ and $P_1(s_*)$; P_0 , z_0 , n_0 are, respectively, the height, base half-width, and the degree of the slope steepness of the principal mountain; P_1 , z_1 , n_1 , and s_{*1} are, respectively, the height, base half-width, the degree of the slope steepness, and the coordinate of the top (separation from the principal mountain) of the neighboring mountain. The profile (12) differs from Eq. (11) by the parameters n_0 and n_1 characterizing the slope steepness of the mountains and by the absence of wing overlapping of the two mountain profiles $P_0(s_*)$ and $P_1(s_*)$. Therefore, Eq. (12) more accurately describes the real mountain profile at the measurement site.

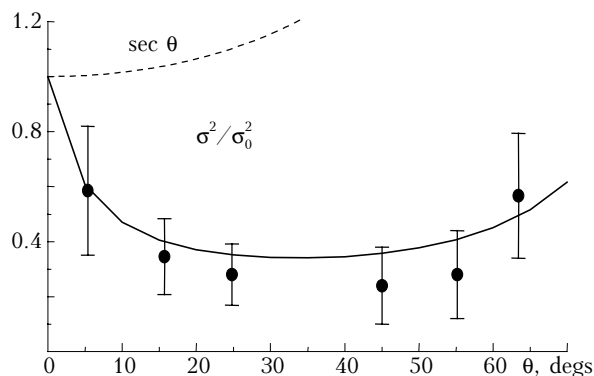


Fig. 6. Effect of mountain terrain on the variance of image jitter of stars. Dots are for the experimental data from Ref. 23, vertical bars show the confidence intervals. Tajikistan, Mount Sanglok, summer of 1960, nighttime measurements, $h_0 \approx 20$ m. The solid curve corresponds to the theoretical results for the parameters of real mountain profile at the measurement site.

From analysis of the real mountain profile near the telescope, the mountain parameters in Eq. (12) can be set as follows: $P_0 = 2237$ m, $z_0 = 250$ m, $n_0 = 1.6$ ($\theta_s \approx 10^\circ$); $P_1 = 1700$ m, $z_1 = 1000$ m, $n_1 = 0.5$, $s_{*1} = 1000$ m. Figure 6 demonstrates the comparison of the theoretical and experimental²³ data.

As can be seen from Fig. 6, the type of the underlying terrain in the region of the observation site should necessarily be taken into account for the correct prediction of the jitter of astronomic images. The allowance for the terrain allows us to explain the discrepancy between the earlier theoretical data and the experimental results that deviate significantly from the secant law (dashed curve).

References

1. V.I. Tatarskii, *Wave Propagation in a Turbulent Medium* (McGraw-Hill, New York, 1961).
2. A.S. Gurvich, A.I. Kon, V.L. Mironov, et al., *Laser Radiation in the Turbulent Atmosphere* (Nauka, Moscow, 1976), 277 pp.
3. I.G. Kolchinskii, *Optical Instability of the Earth's Atmosphere as Judged from Star Observations* (Naukova Dumka, Kiev, 1967), 183 pp.
4. P.V. Shcheglov, *Problems of Optical Astronomy* (Nauka, Moscow, 1980), 272 pp.
5. V.P. Lukin, *Atmospheric Adaptive Optics*, SPIE Press Monograph (SPIE, Bellingham, Wash., 1995).
6. A.I. Kon and V.I. Tatarskii, *Izv. Vyssh. Uchebn. Zaved., Radiofiz.* **8**, No. 5, 870 (1965).
7. A.S. Gurvich and M.A. Kallistratova, *Izv. Vyssh. Uchebn. Zaved., Radiofiz.* **11**, No. 1, 66–74 (1968).
8. B.D. Borisov, V.M. Sazanovich, and S.S. Khmelevtsov, *Izv. Vyssh. Uchebn. Zaved., Ser. Fizika*, No. 1, 103–114 (1969).
9. S.S. Khmelevtsov and R.Sh. Tsyvyk, *Izv. Vyssh. Uchebn. Zaved., Ser. Fizika*, No. 9, 108–116 (1973).
10. V.L. Mironov, V.V. Nosov, and B.N. Chen, *Izv. Vyssh. Uchebn. Zaved., Radiofiz.* **23**, No. 4, 461–469 (1980).
11. V.L. Mironov and V.V. Nosov, *Izv. Vyssh. Uchebn. Zaved., Radiofiz.* **17**, No. 2, 247–252 (1974).
12. A.I. Kon, V.L. Mironov, and V.V. Nosov, *Izv. Vyssh. Uchebn. Zaved., Radiofiz.* **17**, No. 10, 1501–1511 (1974).
13. V.L. Mironov and V.V. Nosov, *J. Opt. Soc. Am.* **67**, No. 8, 1073–1080 (1977).
14. V.L. Mironov, *Laser Beam Propagation in the Turbulent Atmosphere* (Nauka, Novosibirsk, 1981), 386 pp.
15. V.P. Aksenov, A.V. Alekseev, V.A. Banakh, et al., *Atmospheric Impact on Laser Radiation Propagation*, ed. by V.E. Zuev and V.V. Nosov, (TB SB AS USSR, Tomsk, 1987), Vol. II, pp. 247–251.
16. V.L. Mironov, V.V. Nosov, and B.N. Chen, *Izv. Vyssh. Uchebn. Zaved., Radiofiz.* **24**, No. 12, 1467–1471 (1981).
17. V.L. Mironov, V.V. Nosov, and B.N. Chen, in: *Abstracts of Papers at Second All-Union Meeting on Atmospheric Optics* (Tomsk, 1980), pp. 101–103.
18. V.P. Aksenov, V.A. Banakh, and B.N. Chen, *Opt. Atm.* **1**, No. 1, 53–57 (1988).
19. V.E. Zuev, V.A. Banakh, and V.V. Pokasov, *Optics of the Turbulent Atmosphere* (Gidrometeoizdat, Leningrad, 1988), 272 pp.
20. M.S. Belen'kii, G.O. Zadde, V.S. Komarov, et al., *Optical Model of the Atmosphere*, ed. by V.E. Zuev and V.V. Nosov, (TB SB AS USSR, Tomsk, 1987), Vol. I, 225 pp.

21. F.D. Eaton, S.D. Ford, and J.E. Miller, SPIE **4376** 410–416 (2001).
22. V.P. Lukin, E.V. Nosov, and B.V. Fortes, Atmos. Oceanic Opt. **10**, No. 2, 100–106 (1997).
23. N.M. Bronnikova, in: *Optical Instability of the Earth's Atmosphere* (Nauka, Moscow–Leningrad, 1965), pp. 116–121.
24. Sh.P. Darchiya, in: *Atmospheric Optics* (1970), pp. 35–41.
25. O.B. Vasil'ev, *Optical Instability of the Earth's Atmosphere* (Nauka, Moscow–Leningrad, 1965), pp. 40–47.
26. I.V. Shvalagin, I.I. Motrunich, and M.M. Osipenko, in: *Atmospheric Optics* (Nauka, Moscow, 1974), pp. 97–103.
27. Sh.P. Darchiya, V.P. Ivanov, and P.G. Kovadlo, *New Technology in Astronomy* (Nauka, Moscow, 1979), Issue 6, pp. 167–175.
28. Sh.L. Darchiya, Izv. GAO AN SSSR **22**, Issue 4, No. 169, pp. 99–113 (1961).
29. A.Kh. Darchiya, Sh.A. Chmil', and Sh.A. Darchiya, Izv. GAO AN SSSR, No. 165, 52–72 (1960).
30. M.V. Bratiichuk and I.V. Shvalagin, in: *Atmospheric Optics* (Nauka, Moscow, 1968), pp. 186–189.
31. O.P. Vasil'yanovskaya, *Bulletin of the Institute of Astrophysics AS Tadj. SSR* (Dushanbe, 1965), Nos. 39–40, pp. 47–78.
32. Sh.P. Darchiya, in: *Optical Instability of the Earth's Atmosphere* (Nauka, Moscow–Leningrad, 1965), pp. 83–90.
33. K.G. Dzhakusheva, Yu.I. Glushkov, N.V. Mikhailova, V.E. Mozhaeva, and D.A. Rozhkovskii, Tr. Astrophysical Institute AS Kaz. SSR **IV**, 110–116 (1963).